# Limited Bifurcation Asymmetry in Coronary Arterial Tree Models Generated by Constrained Constructive Optimization

Wolfgang Schreiner,*‡ Friederike Neumann,‡ Martin Neumann,§ Rudolf Karch,* Adelheid End,‡ and Susanne M. Roedler‖

From the *Department of Medical Computer Sciences, ‡Department of Cardiothoracic Surgery, §Institute for Experimental Physics, Division of Computational Physics, and ‖Department of Cardiology, University of Vienna, A-1090 Vienna, Austria

ABSTRACT Models of coronary arterial trees are generated by the algorithm of constrained constructive optimization (CCO). In a given perfusion area a binary branching network of straight cylindrical tubes is generated by successively adding terminal segments to the growing structure. In each step the site of connection is chosen according to an optimization target function (total intravascular volume), and in any stage of development the tree fulfills physiologic boundary conditions (constraints involving pressures, flows and bifurcation rules). CCO generates structures which in many aspects resemble real coronary arterial trees, except for very asymmetric bifurcations, occurring when a large branch gives off a tiny terminal segment. In the present work we evaluate an additional constraint within CCO, namely imposing a limit on the asymmetry of bifurcations during the construction process. Model trees are grown with different limits imposed, and the effects on structure are studied both phenomenologically and via statistical descriptors. As the limit to asymmetry is tightened, blood is conveyed to the perfusion sites via detours rather than directly and the comparison with measured data shows the structure to change from a conveying to a delivering type of function. Simultaneously total intravascular volume, surface and sum of segments' lengths increase. It is shown why and how local bifurcation asymmetry is able to determine the global structure of the optimized arterial tree model. Surprisingly, the pressure profile from inlet to terminals, being a functional characteristic, remains unaffected.

KEY WORDS: computer-simulation • models, cardiovascular • coronary circulation • arteries-physiology • optimization

## INTRODUCTION

Assuming that arterial trees fulfill their task in an optimized fashion, one can expect that a procedure involving "optimization" has the potential of inducing model structures closely related to what is found in reality (Cohn, 1955; Thompson, 1952; LaBarbera, 1990). This is the basic idea of constrained constructive optimization (CCO),[1] a computational technique developed to generate optimized models of arterial trees from first principles. Without the input of anatomical data, CCO generates the structure of a tree of tubes by adding segment by segment in a geometrically optimized fashion. Since the growth of such a model is only limited by the computational resources, highly complex models of several thousand segments can easily be generated even on medium scale facilities (Schreiner, 1993).

In previous reports we have described in detail the method of CCO and the choice of physiological parameters (Schreiner and Buxbaum, 1993). Moreover, the generated trees have been analyzed with regard to branching angles, pressure profiles, segment radii, and perfusion inhomogeneity (Bassingthwaighte et al. 1989; Schreiner and Buxbaum, 1993; Schreiner et al. 1994), all of which showed satisfactory agreement with experimental measurements (Zamir and Chee, 1986, 1987).

In the present work we focus on a more refined aspect of CCO-generated trees, namely very small vessels branching off from large segments. This morphometrical detail is considered an artifact of CCO trees, at least in comparison with real coronary artery trees. We analyze the consequences, demonstrate a remedy, and reanalyze the results of an improved CCO-procedure, having a "limit to asymmetry" included.

## METHODS

### *The Method of Constrained Constructive Optimization (CCO)*

*Structure and constraints.* Intending to create a dichotomously branching (binary) tree of cylindrical tubes with $N_{term}$ terminal segments, we first formulate appropriate constraints in order to represent reasonable physiological conditions. To these ends we select a perfusion area within which the model is allowed to evolve. Somewhere along the boundary the site of inlet is adopted, where blood enters via the feeding artery at a perfusion pressure ($p_{perf}$) and a total flow ($Q_{perf}$). "Perfusion sites" are distributed all

Address correspondence to Wolfgang Schreiner, Ph.D., FACA, Department of Medical Computer Sciences, University of Vienna, Spitalgasse 23, A-1090 Vienna, Austria. Fax: 43-1-40400-6677; E-mail: wolfgang.schreiner@akh-wien.ac.at

[1]*Abbreviation used in this paper:* CCO, constrained constructive optimization.

over the perfusion area as evenly as possible, and at each perfusion site the distal end of a "terminal segment" (i.e., a segment not bifurcating into daughters) yields a terminal flow ($Q_{term}$) at the terminal pressure ($p_{term}$) to a microcirculatory black-box (not being modeled in detail). We require equal flows ($Q_{term} = Q_{perf}/N_{term}$) and equal pressure at the entrance into all microcirculatory black-boxes (i.e., at the distal ends of all terminal segments). Moreover, at each bifurcation we require the bifurcation constraint,

$$r_o^{\gamma} = r_1^{\gamma} + r_2^{\gamma}, \tag{1}$$

to be fulfilled, which governs the shrinkage of radii from parent ($r_0$) to daughter segments ($r_1$, $r_2$). $\gamma$ is usually set to 2.55 or 3.00 (Zamir, 1977; Arts et al. 1979; Sherman, 1981; Zamir, 1988). Flow resistance in each segment is assumed to follow Poiseuille's Law (Fung, 1984):

$$R = \frac{8 \cdot \eta \cdot l}{\pi \cdot r^4}, \tag{2}$$

(where $\eta$ = viscosity, $l$ = length, $r$ = radius) and the pressure drop, $\Delta p$, across a segment is computed from the flow $Q$ through that segment:

$$\Delta p = Q \cdot r.$$

The overall resistance of the model tree is computed from serial and parallel aggregation of single segments' resistances.

We note that the above specifications do not require any special structure or geometry of the tree model to be implemented. In fact it is very striking that the segment radii of any binary tree can be chosen so as to fulfill the constraints (Schreiner and Buxbaum, 1993).

The structure of a binary model tree can be specified by first assigning an arbitrary but unique index, $i$, to each segment. Then each segment additionally gets two "pointers" holding the indices of the left and right daughters: $D_i^l$, $D_i^r$. For terminal segments these pointers hold "NIL." Redundantly, we also use a backward pointer $B_i$ to the parent of segment $i$. For the root segment $B_i$ points to a dummy segment with index zero and the geometrical coordinates of the inlet ($B_{i=iroot} = 0$). In the frame of structure, nothing is said about the segment lengths and angles defining the geometry of the tree (specified via the geometrical coordinates for the distal ends of all segments $x(i), y(i), i = 1, \ldots N_{tot}$). However, for any geometry, radii can be scaled to make the tree meet all constraints.

At this stage, optimization is introduced as follows: First we adopt an optimization target function which numerically characterizes the global "optimality of the tree". Several arguments for the selection of such a target have been put forward (Thompson, 1952; Cohn, 1954; Cohn, 1955; Lefevre, 1982; Zamir and Bigelow, 1984) and tried within the frame of CCO (Schreiner et al., 1995). A generally accepted choice is, for example, that a tree should have minimum intravasal volume (Kamiya and Togawa, 1972; Sherman, 1981). Given an arbitrary structure and geometry $\{D_i^l, D_i^r; x(i), y(i); i = 1, \ldots N_{tot}\}$ the implementation of the constraints yields a unique determination of all segment radii. The value of the target function (total volume) can then be computed from radii, $r(i)$, and lengths, $l(i)$, of segments:

$$T = V = \pi \sum_{i=1}^{N_{tot}} l(i)\, r^2(i). \tag{4}$$

Now suppose that the position of segment $i$, specified by the geometrical coordinates $(x(i), y(i))$, is displaced: $x(i) \rightarrow x(i) + \delta x$, $y(i) \rightarrow y(i) + \delta y$. In general, this move will change not only the length of segment $i$ but also the lengths of its daughters and induce corresponding changes in resistances, which violate the above formulated constraints. To reimplement them, segment radii have to be rescaled, which is always possible (as explained above), but concomitantly changes the target function, cf., Eq. 4. This change in target function can be exploited to select those moves ($\delta x$, $\delta y$) which optimize (i.e., minimize) the target function (gradient method of minimization [Fröberg, 1985]). Since this procedure can be applied to all segments of a tree, we are able to geometrically optimize any tree within its given structure (constrained optimization).

*The constructive procedure: optimally adding another terminal segment.* The operations explained so far were based on the assumption that a model tree already exists. Now we consider the constructive element of CCO by explaining how a new terminal segment is added to a given tree. A flow chart of the CCO algorithm is shown in Fig. 1.

CCO starts from a scaled but degenerate tree with one segment, carrying the flow $1 \times Q_{term}$ to some arbitrary location

Do i = 1 to maximum number of terminal segments

**1. Tossing for a new terminal location**

REPEAT
- 1.1 Generate the location for a new terminal segment ($x_{term}$, $y_{term}$) from a Pseudo Random Number Sequence (PRNS).
- 1.2 Distance Criterion: Check if this location is not too close to any of the existing segments (adaptive threshold).

UNTIL (distance criterion is met).

**2. Connection Search**

2.1 Evaluation of connections

FOR all existing segments j ≠ i DO

- 2.1.1. Connect terminal i to segment j, creating a new bifurcation $i_{new}$
- 2.1.2. Geometrically optimize $i_{new}$
- 2.1.3. Perform restriction checks (e.g. segment intersection, segments traversing forbidden areas)
- 2.1.4. Save value of target, geometry (i.e. coordinates) and results of checks in line j of the „connection evaluation table" CET
- 2.1.5. Remove $i_{new}$

END DO

2.2 Selection of optimum connection

- 2.2.1. Restrict CET to connections not violating a criterion → subset $CET_r$
- 2.2.2. IF $CET_r$ = {the empty set} THEN goto 1.
  ELSE
  a) Find connection with optimum target (i.e. connection to segment $j_{opt}$ from $CET_r$)
  b) Permanently adopt connection to $j_{opt}$
  END IF

END DO

FIGURE 1. Flow chart for the algorithm of constrained constructive optimization. The algorithm of CCO is capable of optimizing according to a target function which globally characterizes the degree of optimality of the arterial tree model. In each step of optimization the constraints are fulfilled, particularly in each iteration of the geometric optimization (*2.1.2.*) nested within structural optimization (*Connection Search*). Further details regarding implementation have been published in a previous technical paper (Schreiner and Buxbaum, 1993).

within the perfusion area. Then, segments are added step by step to grow a tree model which fulfills all constraints as well as the criteria of optimality at all stages of its development. The resulting model trees may comprise several thousand segments, combining the fineness of fractal arterial tree models (Levin et al., 1986; West and Goldberger, 1987; Popel et al., 1988; Bassingthwaighte et al. 1989) with the advantage that the structure is optimized and hence perfectly arrangeable in space without intersection of segments. In addition, CCO-generated trees have been shown to have branching angles and pressure profiles which are in satisfying agreement with experimental measurements (Schreiner and Buxbaum, 1993; Schreiner et al., 1994), except for tiny branches emerging from large segments.

In general we set the model parameters so as to represent an arterial tree supplying 100 g of myocardial tissue, corresponding, for instance, to the bed of a human left anterior descending (LAD) coronary artery (Netter, 1983; Schreiner and Buxbaum, 1993). The radius of the perfusion area is set to 5 cm, the perfusion pressure ($p_{perf}$) = 100 mm Hg, and the terminal pressure ($p_{term}$) = 60 mm Hg. To standardize conditions, we further assume a fully vasodilated state [400 ml/(min × 100 g)] and cardiac arrest. Then, in addition to diastole, the period of systole also becomes available for coronary perfusion, which increases flow by ~25%. Hence, we end up with a reasonable reference value of $Q_{perf}$ = 500 ml/min. (Schreiner et al., 1994).

### *Modification of CCO: Limiting Bifurcation Asymmetry*

*Motivation.* There is one feature of CCO trees which deserves attention and remedy: In CCO-trees we find very thin segments branching off from thick mainstream segments. The reason is that CCO does not draw on any quantitative anatomical data and within "pure CCO" no restrictions are implemented precluding such structures. The degree of asymmetry of a bifurcation is usually expressed by the "symmetry index":

$$\xi_{rad} = r_2/r_1,\ 0 < \xi_{rad} \leq 1, \tag{5}$$

where $r_2$ and $r_1$ represent the radii of the small and large daughter segments ($r_2 \leq r_1$). Very asymmetric bifurcations have symmetry indices close to zero, whereas perfectly symmetric bifurcations are characterized by $\xi_{rad} = 1$. Extensive measurements on casts of porcine coronary arteries (van Bavel and Spaan, 1992) have shown that extremely small symmetry indices are rare in real arterial trees. In fact, not a single bifurcation with $\xi_{rad} < 0.05$ was reported to occur within as many as 2,366 segments. In addition we have performed our own measurements on microvascular casts of 439 segments of human coronary arterioles, ranging between 3.5 and 109 μm in radius (Aharinejad, S.H., W. Schreiner, and F. Neumann. 1996. Manuscript submitted for publication). The minimum symmetry index encountered was $\xi_{rad} = 0.21$, and the 5% quantile was as large as 0.51. We therefore conclude that the rather frequent occurrence of heavily asymmetric bifurcations represents an artifact of CCO models. It is simple, however, to modify CCO to avoid such small symmetry indices.

*Imposing a limit on asymmetry.* Extremely asymmetric bifurcations are avoided by one additional check during the "connection search" procedure:

Following optimization, each new bifurcation is subjected to a test of its symmetry index (as part of the restriction checks 2.1.3 in Fig. 1 showing the algorithm). The tentative connection site is only given the chance to be accepted if the symmetry index exceeds a preset threshold ($\xi_{rad} \geq \xi^{low}$); otherwise it is precluded from becoming permanent (item 2.2.1 in the algorithm).

This amendment suppresses very asymmetric bifurcations and thus influences the structural development mainly in the vicinity of large mainstream segments. In these regions, a new terminal site is connected via (a detour along) the smaller branches of a near subtree rather than being directly connected to a large segment, even if the latter is closer. With an increasing value of $\xi^{low}$, the structural changes involve increasing portions of the tree, even in zones remote from mainstream segments, cf. Fig. 2, *A–D.*

On an intuitive basis the structural changes can be described most clearly by focusing on a specific region of interest. We focus on an area immediately below two major branches bifurcating from the mainstream (cf. Fig. 2, the path to the respective terminal sites marked blue) and inspect how the route of blood supply changes from panel *A* to *D*:

*$\xi^{low} = 0$:* Without restriction of asymmetry the microcirculatorial area is supplied via a tiny side branch emerging directly from one of the major branches (note that the bifurcation from the major branch into this side branch has a very low value of $\xi_{rad}$), resulting in a very direct access to the site of supply.

*$\xi^{low} = 0.1$:* With a slight restriction on asymmetry, we observe that most regions in the vicinity of large branches are supplied by small subtrees with approximately four to six terminals. The roots of these subtrees are thick enough to pass the check for asymmetry and thus can directly branch off from one of the major branches. However, the route of blood supply is in most cases slightly longer than in Fig. 2 *A* (passing through the subtree is a small detour).

Similar structural changes can be observed along all major branches of the tree, where single terminals have disappeared. Branches of medium and large size remain unaffected regarding topology and geometry.

*$\xi^{low} = 0.3$:* Imposing a more severe restriction on asymmetry continues the above trend and allows only larger subtrees to emerge from the major branches. Concomitantly the detour to the site of supply becomes larger.

The major branches of the tree still remain more or less unaffected regarding topology and geometry.

*$\xi^{low} = 0.4$:* With this very severe restriction, another additional portion of bifurcations of the tree are forced to be "even more symmetric". The very basic and dramatic changes induced in global structure may in fact be seen as a "switch in topology". In particular, the terminal site on which we have focused above, is now supplied via a totally different subtree emerging from the left (instead of the right) major branch. (Please note that "right" and "left" refers to the direction of blood flow.) The former route of supply is no longer feasible, since the subtree has vanished. Instead, a new subtree has emerged far more distally.

The specific example clearly illustrates how local restrictions on asymmetry can entail global changes in structure. In RESULTS, we shall provide quantitative estimators for the effects intuitively characterized above.

## RESULTS

### *Quantifying the Structural Impact Caused by the Limit to Asymmetry*

The effect of $\xi^{low}$ is not only visually evident (Fig. 2) but can also be easily quantified.

*Bifurcation levels and Strahler orders.* In a binary branching tree, each segment belongs to a certain "bifurcation level," defined by the number of bifurcations along the path from the root of the tree towards the respective segment (Zamir and Chee, 1987). The highest bifurcation level is usually reached by one (or several) of the terminal segments most remote from the root of the tree, and thus also characterizes the tree as a whole. Limiting asymmetry drastically reduced the number of

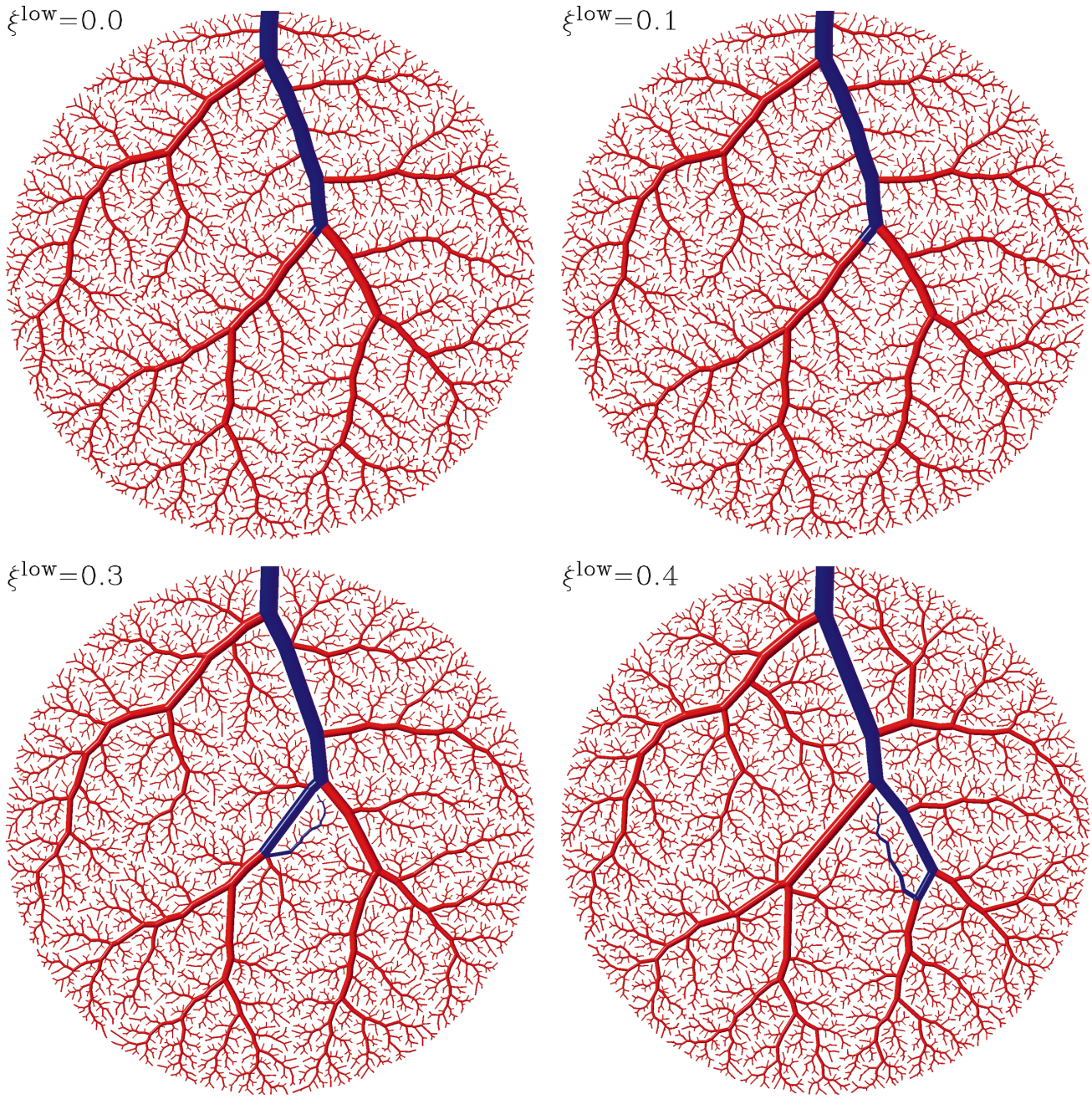


FIGURE 2. Structural changes of CCO-generated arterial tree models due to a limit to asymmetry. All four trees were generated with identical constraints, and the optimization target was minimum intravasal volume. Comparing the trees in panels *A* (upper left), *B* (upper right), *C* (lower left), and *D* (lower right) shows how an increasing restriction on local bifurcation asymmetry changes the global topological and geometrical structure. For a discussion of specific aspects see METHODS.

bifurcation levels from approximately 100 (for $\xi^{low} = 0$) to as few as 28 for $\xi^{low} = 0.4$ (Table I).

Another very useful classification criterion, the Strahler order (Strahler, 1952, 1957), is virtually unaffected by the structural changes induced by $\xi^{low}$ (Table I).

*Frequency distribution of symmetry index.* A CCO-generated tree with $\xi^{low} = 0$, i.e., without restriction on asymmetry, has a typical frequency chart of the symmetry indices displayed in Fig. 3 (*solid curve*), showing very asymmetric bifurcations with $\xi_{rad}$ as low as 0.05. Introducing a limit on asymmetry cuts off the low-value tail of the distribution and diverts new bifurcations towards the right part of the frequency chart. In the plot this effect is reflected by two features:

(*a*) The minimum values of $\xi_{rad}$ are shifted to the right as $\xi^{low}$ increases. Qualitatively this is exactly what

TABLE I

*Dependence of Segment Radii and Number of Bifurcation Levels on the Limit to Asymmetry*

| [mm] $\zeta^{low}$ | $r_{root}$ [mm] | $\frac{\min\{r\}}{r_{root}}$ | Bifurcation levels | Strahler orders |
|---|---|---|---|---|
| 0 | 1.687 | 0.01720 | 0–105 | 0–6 |
| 0.1 | 1.688 | 0.01719 | 0–95 | 0–6 |
| 0.2 | 1.693 | 0.01601 | 0–48 | 0–6 |
| 0.3 | 1.703 | 0.01673 | 0–33 | 0–6 |
| 0.4 | 1.716 | 0.01713 | 0–28 | 0–7 |

The limit to asymmetry, ($\xi^{low}$, [dimensionless]), is defined according to Eq. 5. All radii in CCO-trees are scaled with reference to $r_{root}$ (radius of the root segment). $r_{root}$ itself is then set so as to make the resistance of the whole tree yield the total flow required by the boundary conditions. The root segment has bifurcation level 0. Following any path from root to its terminal segment, the level count is increased by 1 at each bifurcation. According to Strahler's terminology terminal segments are assigned Strahler order 0 (Strahler, 1952, 1957). If both daughters of a bifurcation have unequal Strahler orders, the parent segment acquires the larger Strahler order. If both daughters have Strahler order $j$, the parent segment has Strahler order $j + 1$. The root segment always has the maximum Strahler order occurring in a tree. Successive segments may have equal Strahler orders, whereas they always have different bifurcation levels.

one would expect; quantitatively we have to notice, however, that in the fully developed tree values of $\xi_{rad}$ exist which are smaller than the limit imposed during construction. The explanation for this surprising result is as follows: Even if symmetry indices $\xi_{rad} < \xi^{low}$ are prohibited in the instance of connecting a new terminal, the symmetry index of an existing bifurcation may change later (item 2.1.2 in the algorithm) and violate the limit. This will be the case if the two subtrees supplied by a bifurcation grow at different speeds (e.g., much more terminals are added to the left than to the right subtree). Then segment radii must be adapted so as to maintain a correct splitting of flow, thereby shifting $\xi_{rad}$ (towards asymmetry). Since this process of scaling cannot be subjected to any limitation, it may lead to values of $\xi_{rad}$ (e.g. $\approx 0.16$) well below the corresponding threshold ($\xi^{low} = 0.4$).

(*b*) The modal value of the distribution is stable at $\xi_{rad} = 0.58$ for all choices of $\xi^{low}$. Frequencies left to the mode decrease, while frequencies right to the mode increase as $\xi^{low}$ increases.

*Geometric location of the most asymmetric bifurcations.* Without imposing a limit on asymmetry (Fig. 2 *A*) the most asymmetric bifurcations occur along the main branches when these give off single terminals. When these structures are precluded via $\xi^{low} > 0$, the bifurcations with the lowest symmetry indices become distributed more or less evenly over the tree.

*Limiting asymmetry increases the "path-to-bee-line-ratio."* The detour of blood flow to a given perfusion site, as induced by imposing a limit on asymmetry, can easily be quantified by the ratio between the actual path length of blood transport to a particular terminal segment and the corresponding bee-line (Schreiner et al. 1995). The actual path of blood from the tree's inlet to any specific terminal site traverses a sequence of segments (contained in the set {*path*}) and has a total length:

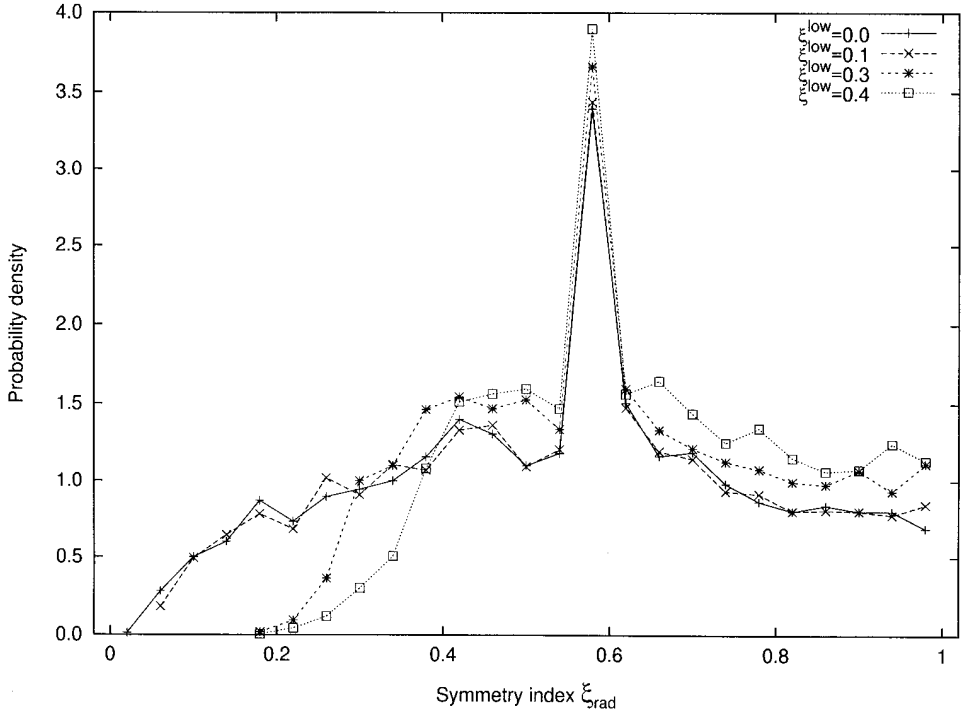


FIGURE 3. Probability density of symmetry index. x-axis: symmetry index ($\xi_{rad}$, [dimensionless]) according to Eq. 5. y-axis: estimated probability density. All trees have 4,000 terminal segments and are optimized for minimum intravasal volume. Note that each (of the 3,999) bifurcating segment(s) has a symmetry index, whereas terminal segments have none. (*solid line*) $\xi^{low} = 0$, i.e., a tree without restriction. See the legend for the other values of $\xi^{low} = 0.1, 0.3, 0.4$, corresponding to the trees shown in Fig. 2.

$$L_{\text{path}} = \sum_{j \varepsilon \{path\}} l(j). \quad (6)$$

The bee-line, being defined as the straight connection between the inlet of the tree and the terminal site ($L_{\text{bee-line}}$) allows to define the "path-to-bee-line-ratio":

$$R_L = L_{\text{path}} / L_{\text{bee-line}}. \quad (7)$$

By definition, $R_L \geq 1$, since the path can never be shorter than the bee-line. In fact, in any tree there are several terminals for which $R_L$ is close to 1. A necessary condition is a very straight arrangement of the segments, not significantly deviating from a common direction, usually that of a mainstream artery (Fig. 4). Generally, the majority of segments show moderate values of $R_L$, whereas a minority of segments have very large values of $R_L$ (the distribution of $R_L$ is right skewed, with the skewness increasing from 1.73 to 12.0 as $\xi^{low}$ increases from 0 to 0.4). The mean values of $R_L$ rise only from 1.23 to 1.53, whereas the maximum values of $R_L$ (characterizing the most severe detour in a tree) increase drastically from 2.13 to 35.8. All these features quantitatively characterize the effect of a restriction on local asymmetry.

*Orientation of terminal segments.* In the CCO-tree with $\xi^{low} = 0$ blood accesses the terminal sites in a rather direct fashion, whereas detours arise with increasing $\xi^{low}$. One can expect that, following a detour, the perfusion site is finally reached from a direction more at random than in the case of a direct access. To investigate this quantitatively, the orientation of each terminal segment is computed relative to the most direct access, namely the orientation of the respective bee-line:

$$\varphi = \arccos \frac{\vec{b} \cdot \vec{s}}{|\vec{b}| \cdot |\vec{s}|}, \quad (8)$$

where $\vec{b}$ and $\vec{s}$ are the vectors of bee line and segment, respectively. Fig. 5 shows the resulting distribution of angles. Surprisingly, almost no difference is noticeable between limited and unlimited asymmetry.

*Dependence of Global Quantities on the Limit to Asymmetry*

The change in structure, characterized by additional detours in reaching the perfusion sites, is accompanied by changes in global morphometric descriptors such as total volume, total surface, and the sum of segment lengths. As local asymmetry is reduced by increasing $\xi^{low}$ from 0 to 0.4, the total volume and total surface rise by ~10 and 8%, respectively (Fig. 6). The sum of segment lengths shows only a very small and random variation (0.7%).

Increasing path lengths requires a concomitant increase in radii so as to keep the total resistance constant. The largest radius within the tree, i.e., that of the root segment, increases by 1.7% when $\xi^{low}$ varies between 0 and 0.4 (see Table I). At the same time, the relation between the radii of the smallest segment of the tree and its root segment remains almost constant (Table I).

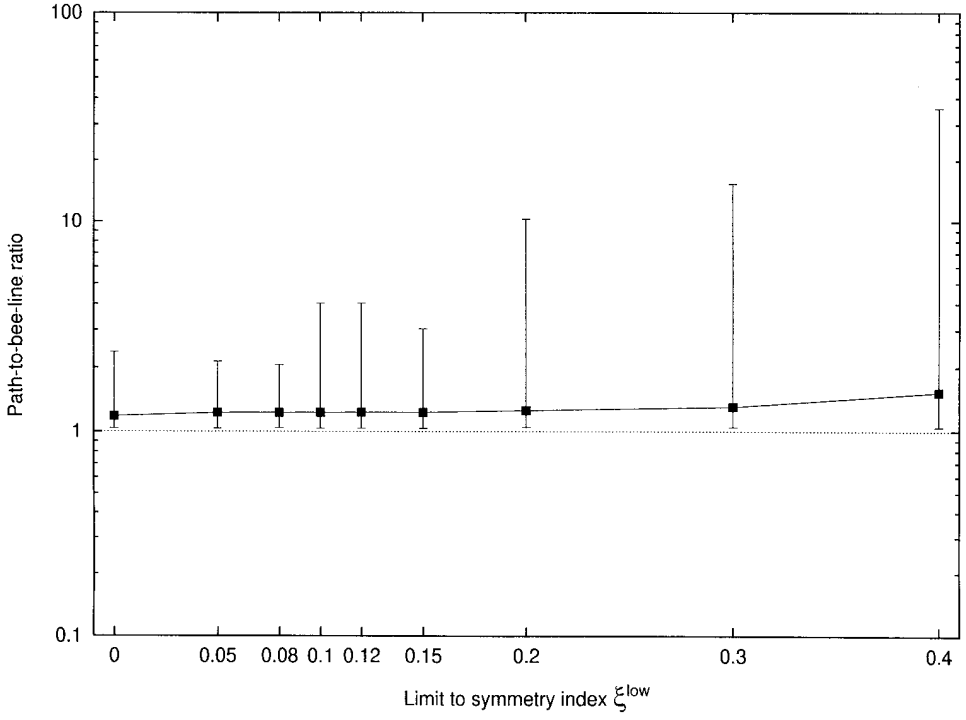


FIGURE 4. Path-to-bee-line ratio for limited asymmetry. x-axis: limit to symmetry index ($\xi^{low}$). y-axis: path-to-bee-line ratio as defined in Eq. 7. For each tree the paths to all terminal segments are examined; squares indicate mean values, bars show minima/maxima. Note that this figure also displays the results for additional CCO-trees with $\xi^{low}$ = 0.05, 0.08, 0.12, 0.14, and 0.2.

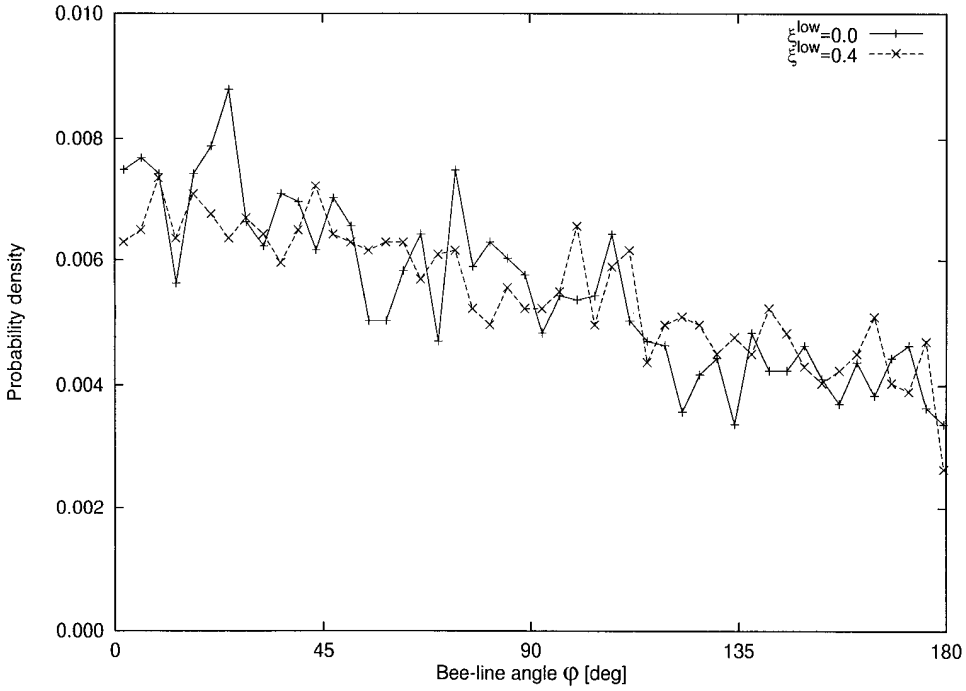


FIGURE 5. Segment direction relative to the bee line. x-axis: angle between bee-line and segment orientation, φ[deg]. y-axis: probability density [deg$^{-1}$]. φ is computed via the scalar product. 0 deg indicates parallel orientation, 180 deg parallel-opposed orientation. (*solid line*) tree with $\xi^{low} = 0$; (*dashed line*) tree with $\xi^{low} = 0.4$.

*Quantifying the Functional Impact Caused by the Limit to Asymmetry*

*Branching rate, conveying and delivering type of function.* Human coronary arteries have been analyzed regarding their "conveying" and "delivering" type of function (Zamir, 1988), which is closely related to bifurcation asymmetry. Conveying vessels are those which accomplish the transport of blood to a remote part of tissue. Along their way they can only "afford" to lose little flow through small side branches and diminish in radius only slightly across such bifurcations. In contrast, delivering vessels bifurcate close to symmetric (thereby severely diminish in radius) and thus yield the whole flow

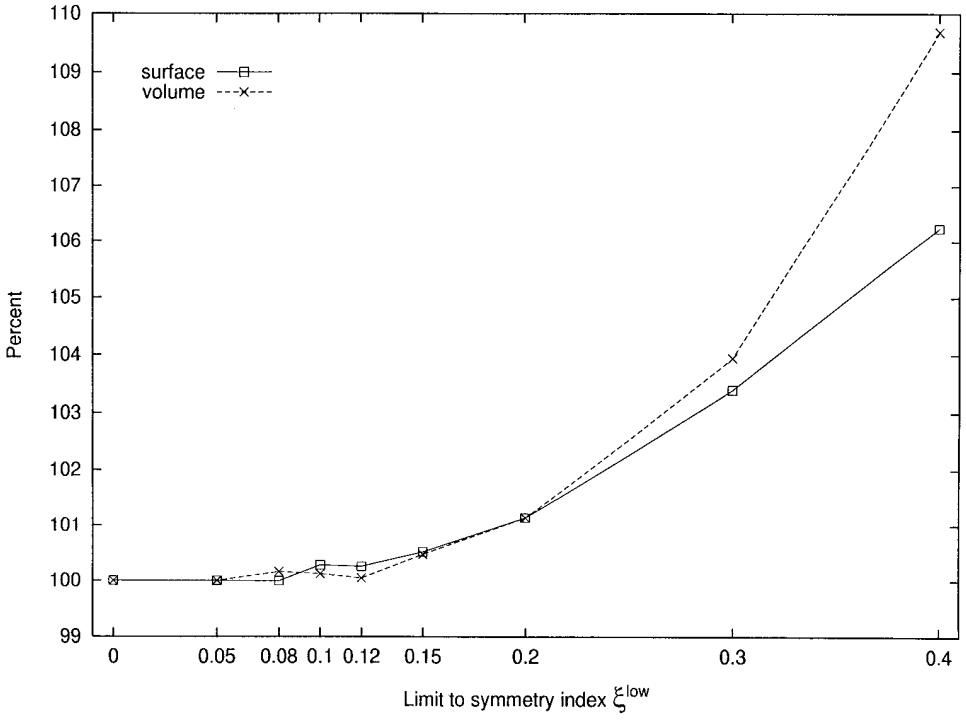


FIGURE 6. Dependence of volume and surface on the limit to asymmetry. x-axis: limit to asymmetry $\xi^{low}$, [dimensionless]. y-axis: percentage relative to reference tree ($\xi^{low} = 0$). Total intravasal volume of tree, shown as crosses, total surface of vessels in the model tree, shown as squares. Note that this figure also displays the results for additional CCO-trees with $\xi^{low} = 0.05$, 0.08, 0.12, 0.14, and 0.2.

carried to the tissue within a short distance. The decline of radius across a bifurcation is described by the "branching rate" (Zamir, 1988):

$$\lambda = r_1/r_0\,, \tag{9}$$

which is related to the symmetry index via Eq. 1:

$$\lambda^\gamma = 1 - \xi_{rad}{}^\gamma. \tag{10}$$

Eq. 10 shows that increasing symmetry ($\xi_{rad}$) is coupled to decreasing branching rate ($\lambda$).

Following the "main path" (i.e., choosing always the larger daughter along a particular path) of a vessel tree, the radius diminishes at each bifurcation according to the respective branching rate $\lambda$. One usually encounters different values of $\lambda$, since the reduction in radius of the main vessel depends on the radius of the branch according to Eq. 10. Eq. 1 is not identically but approximately fulfilled in real trees (Kamiya and Togawa, 1972). If the branching rate were constant, the relative decrease in radius after traversing $n$ bifurcations along a main path would simply be given by:

$$\frac{r_n}{r_0} = \lambda^n. \tag{11}$$

In a semi-log plot over $n$ this ratio appears as a straight (descending) line, the slope of which is given by $\log(\lambda)$. For real coronary trees (Zamir, 1988) and for realistic models the average value of $\lambda$ may be computed via a linear regression.

TABLE II

*Dependence of Branching Rate on the Limit to Asymmetry*

| $\zeta^{low}$ | $\lambda$ | $R^2$ | $\lambda_1$ [cm$^{-1}$] | $R^2$ |
|---|---|---|---|---|
| 0 | 0.978 | 0.909 | −0.0825 | 0.981 |
| 0.1 | 0.974 | 0.939 | −0.0838 | 0.983 |
| 0.2 | 0.947 | 0.986 | −0.0917 | 0.986 |
| 0.3 | 0.904 | 0.993 | −0.0917 | 0.976 |
| 0.4 | 0.883 | 0.995 | −0.1009 | 0.985 |

For each value of $\zeta^{low}$ the average branching rate $\lambda$ along the "main path" of each tree was computed from the slope of a linear regression of $\log(r_n/r_0)$ versus $n$, cf. Eq. 11. These regressions against the structural variable $n$ were seen to discriminate well between trees. Conversely, regressions for $r_n/r_0$ over the metric path lengths (regression slope $\lambda_1$) failed to discriminate between trees. $R^2$ is the ratio of explained variance (i.e., $R^2$ = Sum of Squares (Model)/Sum of Squares (total), used as the criterion for the goodness of fit.

It is now very interesting to compare experimental measurements on the branching rate (Zamir, 1988) with the results obtained from the CCO-model. We extracted the radii of successive segments along the "main branch" of each CCO-tree and plotted the ratio of segment radius and radius of the root in a semi-log plot over the bifurcation level (Fig. 7).

Linear regressions were computed according to least squares, and the corresponding values of $\lambda$ (computed from the regression coefficient) are given in Table II.

The CCO-tree without a limit to asymmetry shows the slowest decline in radius with ($\lambda = 0.978$; this means that on the average the larger daughter of a bifurcation shrinks

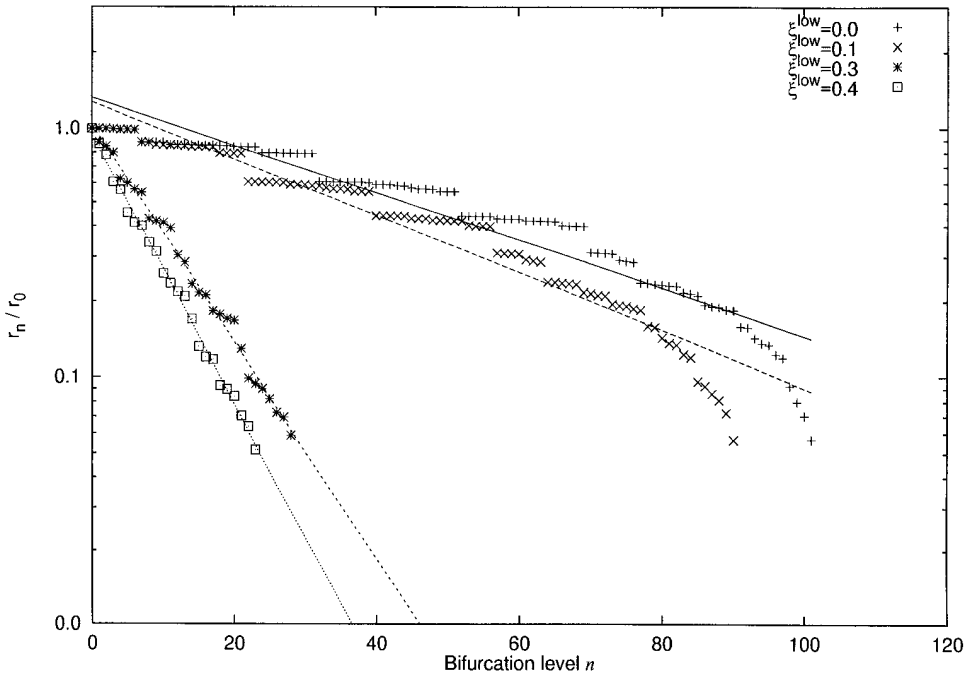


FIGURE 7. Branching rate for "main path" in CCO model. x-axis: bifurcation level $n$. y-axis: $r_n/r_0$. For symbols see figure legend. For each $\xi^{low}$ a separate linear regression for $\log(r_n/r_0)$ over $n$ has been performed according to least squares. The branching rates, computed from the regression coefficients and characterizing the shrinkage of segment radius are given in Table II, compare also Eq. 11.

to 97.8% of the parent's radius. According to experimental work (Zamir, 1988), where vessels with $\lambda > 0.96$ are classified as conveying, this CCO-tree definitely belongs to the conveying or "distributing" type of vessel.

If bifurcation asymmetry is increasingly limited, the radii along the main path diminish more rapidly (Fig. 7). The corresponding branching rate declines to $\lambda = 0.883$ for $\xi^{lim} = 0.4$, thus classifying the main path of this tree as a delivering vessel in terms of experimental data (Zamir, 1988).

The same is true for the flow carried by the segments along the main path: With unlimited asymmetry the flow decreases in numerous small steps due to the flow loss into small side branches, bifurcating from the main path in close succession. With a limit to asymmetry, about the same average flow loss per unit path length is observed, however flow decreases in fewer but more pronounced steps.

It is important to notice that the branching rate is solely defined on a structural basis (bifurcation levels) whereas actual segment lengths are completely ignored. It is interesting to show that this structural approach is able to discriminate between conveying and delivering types of vessels whereas a "metric approach," using segment lengths, is not. Therefore we also plot $\lambda$ against the (metric quantity) path length (Fig. 8) rather than against the bifurcation level. The decline in radius with reference to the root is approximately linear in path length, but regressions show very similar slopes ($\lambda_l$) and are unable to discriminate between trees (Table II).

*Pressure profile and bifurcation asymmetry.* To obtain the pressure profile over a CCO model tree we consider the pressure at the distal end as representative for the whole segment. For any segment, $p_{dist}$ can be computed by adding up the segmental pressure gradients along the path from the root to the respective segment:

$$p_{dist,i} = p_{perf} + \sum_{i \epsilon path} \Delta p_i \, . \qquad (12)$$

Specifically for terminal segments, summing up segmental pressure gradients identically yields the unique terminal pressure, $p_{term}$, which enters the model as a constraint.

To obtain the pressure profile, pressures of single segments are usually grouped into classes equidistantly spaced in the logarithm of segment radius (Chilian et al. 1990). In such a semi-log plot, the pressure profile of a real arterial tree should appear close to a straight line (van Beek et al. 1989). The fact that the CCO model reproduces this feature nicely (Fig. 9) is an additional confirmation of model adequacy.

With regard to bifurcation asymmetry, we were surprised to find that the pressure profiles are almost identical for the CCO-tree with unlimited asymmetry ($\xi^{low} = 0$) and the tree with $\xi^{low} = 0.4$, despite the markedly different structures of these trees.

In the range of very small radii, an increasing number of terminal segments contribute to the pressure average of each class, and for $r \leq 0.06$ mm there are exclusively terminals. They all contribute the unique pres-

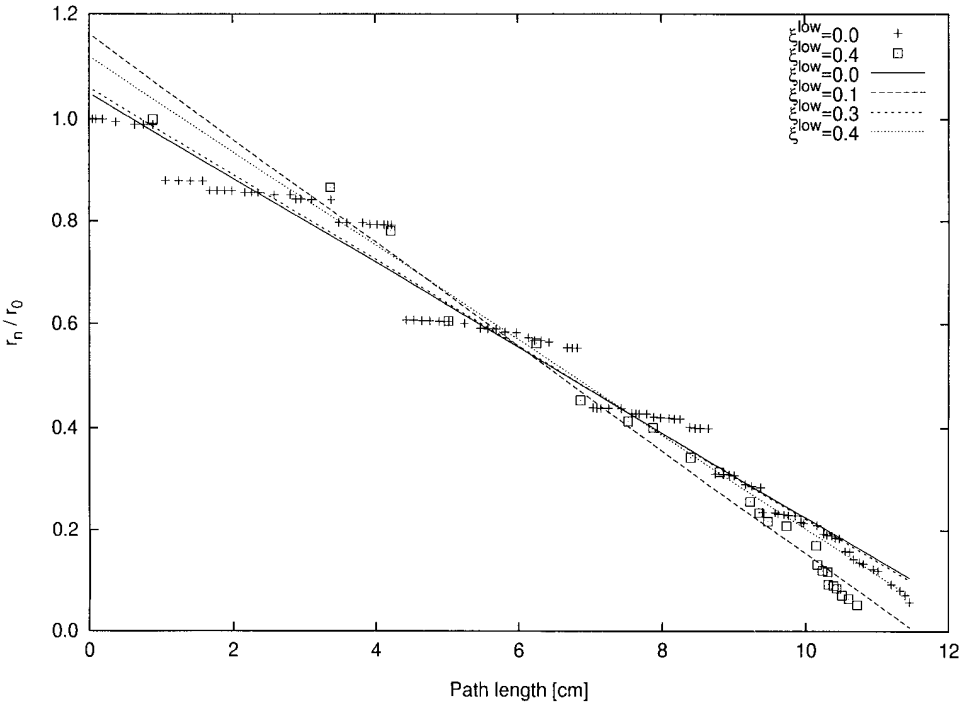


FIGURE 8. Modified definition of branching rate based on path length. x-axis: path length (cm) from root along the main path towards the terminal. The main path is traced by bifurcating into the larger daughter when crossing a bifurcation. y-axis: $r_n/r_0$. For each $\xi^{low}$ a separate linear regression for $r_n/r_0$ over path lengths has been performed according to least squares. Regression coefficients are given in Table II.

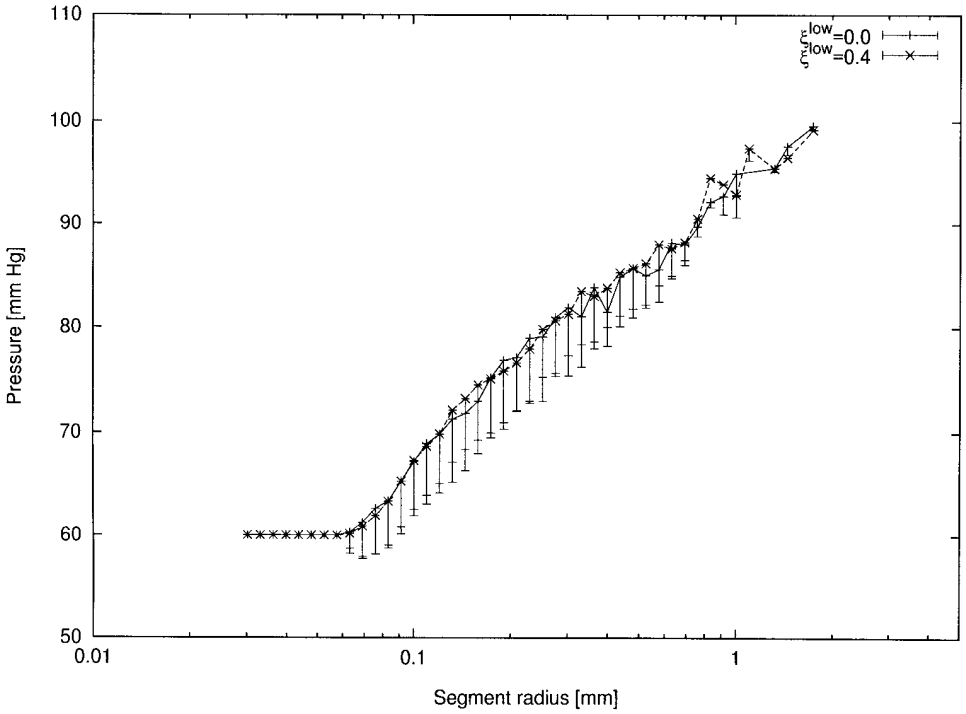


FIGURE 9. Insensitivity of pressure profiles to the limit to asymmetry. x-axis: segment radius (mm). y-axis: pressure (mm Hg) at distal end of segment. Symbols denote mean values and bars standard deviations. (*solid line*) tree without a limit on asymmetry (Fig. 2 *A*); (*dashed line*) tree with $\xi^{low} = 0.4$ (tree shown in Fig. 2 *D*).

sure ($p_{term}$ = 60 mm Hg), and hence the spread is zero (error bars coincide with mean values).

## DISCUSSION

CCO generates the structure and geometry of arterial tree models without drawing on any information from topographic anatomy. Yet the models resemble real coronary arterial trees in many features, as discussed and evaluated in previous reports (Schreiner and Buxbaum, 1993; Schreiner et al., 1994; Schreiner et al., 1995). However, the existence of very small side branches emerging from big vessels is conspicuous (Fig. 2 *A*) when compared with real coronary trees, where these structures are rarely found. Therefore we added an additional constraint to CCO by limiting the asymmetry of any new bifurcation when the tree is generated. The resulting changes in structure are not only obvious to visual inspection (detours emerge as a consequence of avoiding highly asymmetric bifurcations, see Fig. 2, *B–D*) but can also be quantified by a set of statistical descriptors.

In the literature the asymmetry of bifurcations has also been related to the functional capabilities of coronary arteries (Zamir, 1988). Asymmetric bifurcations only give off small side-branches and allow the vessel to convey blood across larger distances, which may allow for a large number of bifurcation levels along such a vessel. In contrast, symmetrically bifurcating vessel trees readily deliver blood to the tissue and reach the terminal level after only a few bifurcation levels. These functional differences are most clearly reflected in the branching rate analysis. First, the low number of bifurcation levels in "more symmetric trees" most naturally leads to a more rapid decline in radius (see Fig. 7). The low spread of data around the regression line proves that the trees with a severe limit on asymmetry exhibit almost constant branching rates. The result for the tree without a limit on asymmetry is completely different: in the large-caliber region of its main path we observe several series of consecutive segments, with radii decreasing only slightly within each series. This is due to very small but numerous side branches, each leaving the radius of the continuing main-stream vessel almost unaffected. Two adjacent series are divided by a distinct downward step in radius, corresponding to a more prominent sidebranch. Thus the slope of the regression line represents only the average decline in radius, resulting in lower values of $R^2$ (cf., Table II). Moreover, the peripheral part of the main path shows a markedly steeper slope in the semi-log plot, indicating that bifurcations become more and more symmetric. In fact, the local slope for bifurcations beyond a level of 80 is similar to that found for $\xi^{low} = 0.4$.

The interpretation of these results and the comparison with measured data taken from the literature (Zamir, 1988) shows that, in terms of Zamir's definition (Zamir, 1988), CCO-models have been turned from conveying to delivering by imposing a limit on asymmetry.

Another descriptor most directly affected is the probability distribution of $\xi_{rad}$, which is skewed towards

larger values while its modal value remains constant as $\xi^{low}$ increases (Fig. 3). We recall the striking observation that during further growth of the tree, existing bifurcations may be diverted towards asymmetry, even beyond the limit valid for newly generated ones.

Simultaneously with the probability distribution, the geometrical and topological locations of the most asymmetric bifurcations in the tree change: for $\xi^{low} = 0$ these are concentrated along the major branches whereas for $\xi^{low} = 0.4$ the most asymmetric bifurcations are randomly distributed over the tree.

The "amount of detours" itself was characterized by the path-to-bee-line-ratio (Fig. 4). Imposing a limit on asymmetry increases the "mean amount of detours" only moderately (from 1.23 for $\xi^{low} = 0$ to 1.53 for $\xi^{low} = 0.4$, i.e., by a factor of $1.53/1.23 = 1.24$) whereas the most excessive detours increase drastically in length (from 2.13 to 35.8, respectively, i.e., by a factor of $35.8/2.13 = 16.8$).

The effects of the limit to asymmetry on global quantities is easily understood by considering the implications of detours replacing the straight access: (*a*) detours lengthen the paths and thus directly increase the total sum of segment lengths. Since total surface and volume are both proportional to segment lengths ($S \propto l \cdot r$, $V \propto l \cdot r^2$), they also increase (Fig. 6). (*b*) Despite longer paths the total resistance to flow (according to Poiseuille's law [Fung, 1984]) must remain constant ($R \propto l/r^4$), so as to fulfill the boundary conditions. This is only possible if radii increase (to compensate for increasing lengths). This contributes a second factor to the growth in surface and volume (proportional to $r$ and $r^2$, respectively), which together with the effect of segment lengths, yields increases of 8 and 10%, respectively.

The pressure profile from the inlet to the terminal segments of the tree was found to be almost unaffected by the structural changes induced by limited asymmetry (Fig. 9). This finding parallels a result found earlier, namely that the structural changes induced by different optimization targets do not influence the pressure profile either (Schreiner et al., 1995). We may therefore conclude that structural changes on the whole do not severely influence the pressure profile.

The horizontal portion belonging exclusively to terminal segments ($r \leq 0.06$ mm) is certainly an artifact due to the need to truncate the model tree distally (to keep the total number of segments within computational resources). In other words, the pressure profile offers a glimpse of "boundary conditions artifacts," which may be evaluated by considering CCO trees of increasing resolution in coming studies. From the present work we can draw the preliminary conclusion that predictions regarding pressures or flows are only reliable if one keeps off from terminal segments (and probably from their immediate parents as well).

The main result of the present work was to show qualitatively and quantitatively why and how a local restriction on asymmetry is able to influence the global structure of optimized arterial tree models.

---

The authors wish to thank Mrs. E. Sumetzberger for preparing the manuscript.

This work was supported by the Bundesministerium für Wissenschaft und Forschung, grant 49.820/4-24/92.

*Original version received 12 June 1996 and accepted version received 16 October 1996.*

## REFERENCES

Arts, T., R.T.I. Kruger, W. van Gerven, J.A.C. Lambregts, and R.S. Reneman. 1979. Propagation velocity and reflection of pressure waves in the canine coronary artery. *Am. J. Physiol.* 237:H469–H474.

Bassingthwaighte, J.B., R.B. King, and S.A. Roger. 1989. Fractal nature of regional myocardial blood flow heterogeneity. *Circ. Res.* 65:578–590.

Chilian, W.M., S.M. Layne, and S.H. Nellis. 1990. Microvascular pressure profiles in the left and right coronary circulations. *In* Coronary Circulation: Basic Mechanism and Clinical Relevance. F. Kajiya, G.A. Klassen, and J.A.E. Spaan, editors. Springer-Verlag, Tokyo/Berlin/Heidelberg/New York. 173–190.

Cohn, D.L. 1954. Optimal systems: I. The vascular system. *Bull. Math. Biophys.* 16:59–74.

Cohn, D.L. 1955. Optimal systems: II. The cardiovascular system. *Bull. Math. Biophys.* 17:219–227.

Fröberg, C.E. 1985. Numerical mathematics. Theory and computer applications. Benjamin/Cummings, Menlo Park, CA. 184–186.

Fung, Y.C. 1984. Biodynamics: Circulation. Springer-Verlag, New York/Berlin/Heidelberg/Tokyo. 84.

Kamiya, A., and T. Togawa. 1972. Optimal branching structure of the vascular tree. *Bull. Math. Biophys.* 34:431–438.

LaBarbera, M. 1990. Principles of design of fluid transport systems in zoology. *Science (Wash. DC).* 249:992–999.

Lefevre, J. 1982. Teleonomical representation of the pulmonary arterial bed of the dog by a fractal tree. *In* Cardiovascular System Dynamics: Models and Measurements. T. Kenner, R. Busse, and H. Hinghofer-Szalkay, editors. Plenum Press, New York/London. 137–146.

Levin, M., B. Dawant, and A.S. Popel. 1986. Effect of dispersion of vessel diameters and lengths in stochastic networks II. Modeling of microvascular hematocrit distribution. *Microvasc. Res.* 31:223–234.

Netter, F.H. 1983. Heart: The Ciba Collection of Medical Illustrations. Thieme-Verlag, Stuttgart/New York. 16–17.

Popel, A.S., A. Liu, B. Dawant, A. Koller, and P.C. Johnson. 1988. Distribution of vascular resistance in terminal arteriolar networks of cat sartorius muscle. *Am. J. Physiol.* 254:H1149–H1156.

Schreiner, W. 1993. Computer generation of complex arterial tree models. *J. Biomed. Eng.* 15:148–150.

Schreiner, W., and P.F. Buxbaum. 1993. Computer-optimization of vascular trees. *IEEE (Inst. Electr. Electron. Eng.) Trans. Biomed. Eng.* 40:482–491.

Schreiner, W., F. Neumann, M. Neumann, A. End, S.M. Roedler, and S.H. Aharinejad. 1995. The influence of optimization target selection on the structure of arterial tree models generated by constrained constructive optimization. *J. Gen. Physiol.* 106:583–599.

Schreiner, W., M. Neumann, F. Neumann, S.M. Roedler, A. End, P.F. Buxbaum, M.R. Müller, and P. Spieckermann. 1994. The branching angles in computer-generated optimized models of arterial trees. *J. Gen. Physiol.* 103:975–989.

Sherman, T.F. 1981. On connecting large vessels to small: the meaning of MURRAY's law. *J. Gen. Physiol.* 78:431–453.

Strahler, A.N. 1952. Hypsometric (area altitude) analysis of erosional topology. *Bull. Geol. Soc. Am.* 63:1117–1142.

Strahler, A.N. 1957. Quantitative analysis of watershed geomorphology. *Trans. Am. Geophys. Union.* 38:913–920.

Thompson, D.W. 1952. On Growth and Form. Volume II. University Press, Cambridge. 948–957.

van Bavel, E., and J.A.E. Spaan. 1992. Branching patterns in the porcine coronary arterial tree. Estimation of flow heterogeneity. *Circ. Res.* 71:1200–1212.

van Beek, J.H.G.M., S.A. Roger, and J.B. Bassingthwaighte. 1989. Regional myocardial flow heterogeneity explained with fractal networks. *Am. J. Physiol.* 257:H1670–H1680.

West, B.J., and A.L. Goldberger. 1987. Physiology in fractal dimensions. *Am. Sci.* 75:354–364.

Zamir, M. 1977. Shear forces and blood vessel radii in the cardiovascular system. *J. Gen. Physiol.* 69:449–461.

Zamir, M. 1988. Distributing and delivering vessels of the human heart. *J. Gen. Physiol.* 91:725–735.

Zamir, M., and D.C. Bigelow. 1984. Cost of departure from optimality in arterial branching. *J. Theor. Biol.* 109:401–409.

Zamir, M., and H. Chee. 1986. Branching characteristics of human coronary arteries. *Can. J. Physiol. Pharmacol.* 64:661–668.

Zamir, M., and H. Chee. 1987. Segment analysis of human coronary arteries. *Blood Vessels.* 24:76–84.